Nanotechnology 23 (2012) 135702 (7pp) doi:10.1088/0957-4484/23/13/135702

Effect of downscaling nano-copper interconnects on the microstructure revealed by high resolution TEM-orientation-mapping

K J Ganesh[1], A D Darbal[2], S Rajasekhara[1], G S Rohrer[2], K Barmak[2] and P J Ferreira[1,3]

[1] Materials Science and Engineering, The University of Texas at Austin, 1 University Station, C2200, Austin, TX 78712, USA

[2] Materials Research Science and Engineering Center, Carnegie Mellon University, 5000 Forbes Avenue, Pittsburgh, PA 15213, USA

E-mail: ferreira@mail.utexas.edu

Received 14 December 2011
Published 14 March 2012
Online at stacks.iop.org/Nano/23/135702

Abstract

In this work, a recently developed electron diffraction technique called diffraction scanning transmission electron microscopy (D-STEM) is coupled with precession electron microscopy to obtain quantitative local texture information in damascene copper interconnects (1.8 μm–70 nm in width) with a spatial resolution of less than 5 nm. Misorientation and trace analysis is performed to investigate the grain boundary distribution in these lines. The results reveal strong variations in texture and grain boundary distribution of the copper lines upon downscaling. Lines of width 1.8 μm exhibit a strong $\langle 111 \rangle$ normal texture and comprise large micron-size grains. Upon downscaling to 180 nm, a $\{111\}\langle 110 \rangle$ bi-axial texture has been observed. In contrast, narrower lines of widths 120 and 70 nm reveal sidewall growth of $\{111\}$ grains and a dominant $\langle 110 \rangle$ normal texture. The microstructure in these lines comprises clusters of small grains separated by high angle boundaries in the vicinity of large grains. The fraction of coherent twin boundaries also reduces with decreasing line width.

(Some figures may appear in colour only in the online journal)

1. Introduction

The scaling required to accommodate faster chip performance in electronic devices has necessitated a simultaneous reduction in the dimensions of copper interconnect (CI) lines fabricated by the damascene process [1–5]. This constant downscaling of CIs has resulted in changes to their microstructure. Among these changes, variations in local texture and grain boundary types are known to strongly affect resistivity [6, 7] and mechanical reliability [8–12]. For instance, strong $\langle 111 \rangle$ fiber textured CIs have been found to exhibit longer electromigration lifetimes when compared to those with a random texture [13]. The electrical and mechanical properties of nanocrystalline materials are strongly influenced by the grain size and density of grain boundaries [14, 15]. In particular, it has been shown that grain boundary scattering is the dominant scattering mechanism in nanometric Cu [14]. Furthermore, grain boundary misorientations also affect the distribution of local stresses in CIs [16].

These aforementioned issues make it critical to understand the impact of downscaling on local texture and the distribution of grain boundary types present in CIs.

[3] Address for correspondence: Department of Mechanical Engineering, The University of Texas at Austin, 1 University Station, C2200, Austin, TX 78712, USA.

 © 2012 IOP Publishing Ltd Printed in the UK & the USA

Conventionally, Kikuchi patterns using electron backscatter diffraction (EBSD) have been used for this purpose. Kim *et al* [17] and Lee *et al* [18] performed microstructure analysis of Cu lines with widths ranging from 0.18 to 2 μm using EBSD and observed the presence of near bamboo-type grains with varying degrees of $\langle 111 \rangle$ fiber texture. Besser *et al* [19] employed XRD and EBSD techniques to determine the effects of line width on textural and microstructural evolution in CIs of similar line widths and observed dominant $\{111\}\langle 110 \rangle$ texture with a more developed $\langle 110 \rangle$ component along the line length in 2 μm-wide lines. Additionally, experiments were carried out by Lee *et al* [20] and Field *et al* [21] to investigate microstructure–reliability relationships in wide CI lines.

Although significant research has been carried out to analyze the microstructure of electrodeposited copper lines, a limited amount of information is available for narrower lines ($\leq$120 nm) consisting of a number of grains smaller than 50 nm in size. This is primarily due to limitations in spatial resolution for determining crystal orientations from a large ensemble of nanocrystalline grains in an automated fashion. Only recently, Legros *et al* [22, 23] have demonstrated morphological evolution through annealing, on in-house fabricated CI lines, down to 80 nm line width using TEM. However, the effect of downscaling on texture and grain boundaries in actual industry-produced CIs found in semiconductor metallization is still unclear. Furthermore, as CIs continue to be downscaled, the spatial resolution of 20 nm employed in the aforementioned work [22, 23] is insufficient to obtain local texture from small grains. In this context, an in-depth analysis of these CIs with statistically significant data is critical to enable microstructure control for improved device designs, materials and processes in future metallization technologies.

In the current work, we use a high resolution orientation-mapping technique in a transmission electron microscope (TEM) to understand the effects of downscaling on the local texture and grain boundaries in damascene CIs. In particular, we have coupled a recently developed diffraction scanning transmission electron microscopy (D-STEM) technique [24] with precession electron microscopy [25–27], using the DigiSTAR$^{\mathrm{TM}}$ system from NanoMEGAS, to comprehensively analyze grain orientations in CIs ranging from 1.8 μm to 70 nm in width with a spatial resolution of <5 nm. The combination of D-STEM and precession microscopy enables: (i) rapid acquisition (at least ten times faster than the original D-STEM technique) of indexable near-kinematical diffraction patterns, with an electron probe of <5 nm, from grains oriented on or off a prominent zone axis with respect to the electron beam direction, and from regions with a high density of defects; and (ii) more reliable automated pattern-indexing due to the presence of higher order reflections, thereby accounting for the 180° ambiguity caused by reflections from planes belonging to one low-index zone axis [28, 29]. Furthermore, we have investigated the presence of coherent $\Sigma 3$ boundaries, non-coincident site lattice (CSL) high angle boundaries and low angle boundaries in CIs with varying line widths from the orientation data by analyzing the grain boundary misorientation and trace orientation [30].

Table 1. Dimensional specifications of damascene Cu specimens of varying line width.

Line width (nm)	Trench depth (nm)	Capping layer thickness (nm)
1800	260	50
180	260	50
120	200	20
70	144	15

2. Experimental procedure

2.1. Sample preparation

Periodic Cu interconnects with line widths of 1.8 μm, 180 and 120 nm were fabricated using the damascene process by Freescale Semiconductor, Inc. The 70 nm wide periodic damascene Cu lines were obtained from Texas Instruments, Inc. The thickness of the underlying Si wafer was 750 μm. Fluorinated tetra-ethyl orthosilicate (F-TEOS) was deposited as the interlayer dielectric (ILD) material for the 1.8 μm and 180 nm wide lines. The 120 nm wide lines were embedded in a carbon-doped oxide (SiCOH) dielectric, while the 70 nm lines were separated by a porous SiCOH dielectric. Ta was used as the diffusion barrier layer for the Cu lines. The electrodeposited Cu along with the overburden layer was annealed at 250 °C for 30 min before the chemical mechanical planarization (CMP) process. Subsequently, the silicon carbon nitride (SiCN) capping layer was deposited by chemical vapor deposition (CVD). The dimensional specifications of the different layers are shown in table 1. TEM samples for planar view observations were prepared by polishing, dimpling and Ar ion milling. To minimize changes in the microstructure during sample preparation, the ion milling process was carried out at low temperatures with a cold stage using low voltages (<3 kV). Samples for cross section examination were prepared by the focused ion beam (FIB) process.

2.2. Electron microscopy

A D-STEM-like lens configuration was employed in a 200 kV JEOL 2010F TEM/STEM to obtain a nano-sized (<5 nm) near-parallel illumination on the specimen. The details of the technique are described elsewhere [20]. The scanning and precession alignments of the beam were controlled using a dedicated unit called DigiSTAR$^{\mathrm{TM}}$, through external connections to the amplifiers of the beam and intermediate deflector coil control boards of the microscope. The nano-probe was precessed and subsequently scanned on the specimen with a step size of 5 nm to obtain sequential diffraction patterns from each pixel. A high frame rate optical camera was employed to collect the patterns during precession, while the intensities from each pixel during scanning were integrated to yield stacks of diffraction patterns with near-kinematical intensities. The precession angle for all acquisitions was set at 0.60°. The obtained diffraction

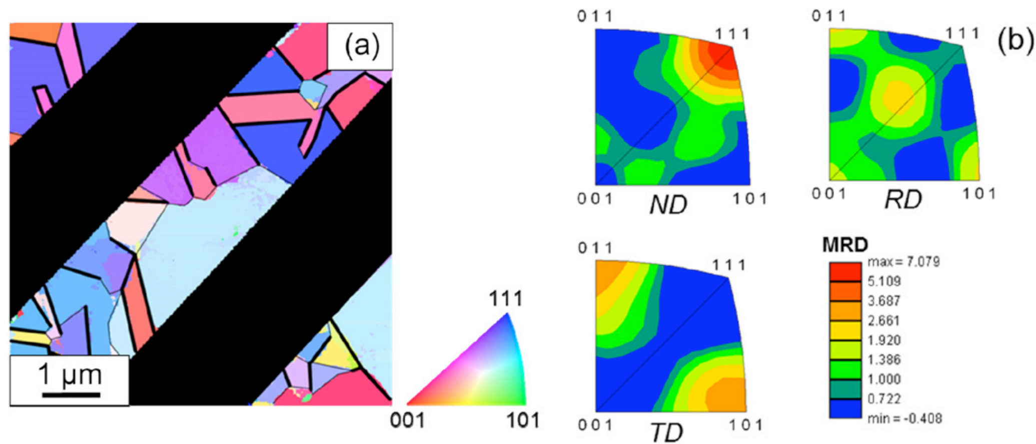

Figure 1. (a) Color coded inverse pole figure (IPF) map from 1.8 μm wide Cu lines. Color codes for orientations are represented in the standard stereographic triangle. (b) Inverse pole figure plots (IPP) along the normal direction (ND), perpendicular to the sample plane, reference direction (RD), along the length of the line and transverse direction (TD), along the width of the line.

patterns were cross-correlated with simulated templates for all possible orientations in Cu within 1° accuracy and assigned correlation index parameters. Each diffraction pattern was assigned a particular orientation based on the template corresponding to the highest correlation index [27]. Prior to the acquisition, calibrations accounting for π-inversion effects in the microscope were performed using an orthorhombic single crystal of α-MoO_3. Subsequently, azimuthal rotation of the patterns was calibrated to set the microscope frame of reference using a thin Cu film sample by matching the trace of the twin boundaries in the orientation map with the twin plane. Orientation data obtained from the scanned region was parameterized in terms of Bunge–Euler angles for quantitative texture analysis. The TSL software was used to bin the parameterized diffraction data and fit series of generalized spherical harmonics to obtain orientation distribution functions. The detailed procedure is described elsewhere [30, 31]. Since the inertial frame of reference of the patterns acquired in the TEM is different from that in the TSL system, active rotation of the parameterized data sets was performed to establish consistency between the frames of reference. The quantitative texture plots thus obtained were expressed in units of multiples of random (MRD) such that an MRD value of 1 indicates the population expected in a random distribution of orientations. For textures with low MRD values, the exact positions of the contours are influenced by the numerical truncation of the harmonic series and do not always reflect the actual symmetry of the system. Finally, misorientation between grains and the trace of the grain boundaries was analyzed to investigate coherent $\Sigma 3^n$ (n = 1–3), low angle and non-CSL high angle boundaries. For adjacent grains satisfying a particular CSL misorientation axis/angle relationship, the trace of the coherency plane in both the grains was matched with the trace of the shared grain boundary to test for coherency of the CSL boundary. The conditions of coherency were set according to Brandon's criterion [32] with a tolerance of 8.7° for the misorientation and 10° for the grain boundary trace orientation. Furthermore, the minimum misorientation tolerance between grains to share a boundary was set at 2°. Therefore, low angle boundaries between grains misoriented by less than 2° were not included in the calculations.

3. Results and discussion

Microstructure observations on 1.8 μm wide periodic damascene CIs showed the presence of large micron-sized grains with a number of twins. A representative color coded inverse pole figure map overlaid with the reconstructed grain boundaries is shown in figure 1(a). Here, RD and TD refer to directions along the length and width of the CI line while ND refers to the out-of-plane normal direction. The colors in the map depict grain orientations along ND, consistent with the color coded standard stereographic triangle. Inverse pole plots (figure 1(b)) obtained from four different sets of samples revealed a strong fiber $\langle 111\rangle$ texture $\parallel$ ND with a slightly mixed $\langle 110\rangle$ and $\langle 112\rangle$ texture also observed along the line length (RD). This observation is consistent with the fact that for $\langle 111\rangle$ texture $\parallel$ ND, the directions in the $\langle 111\rangle$ zone are favored along RD, and these lie along the great circle connecting $\langle 110\rangle$ and $\langle 112\rangle$. Analysis of grain boundary misorientations from a data set of 8000 boundaries from the 1.8 μm lines shows that 42% (length fraction) of the boundaries were of the $\Sigma 3$ type. Among these, more than 98% by length were coherent. The fraction of coherent $\Sigma 3$ boundaries was determined by matching the trace of the grain boundary with the trace of the $\{111\}$ plane. However, it should be noted that the matching between the trace of the grain boundary plane and the $\{111\}$ is a necessary but not sufficient condition for a twin boundary to be coherent. This is because the trace of the boundary plane matches the trace of all the planes whose normals are perpendicular to the boundary line segment. Therefore, the true fraction of coherent twin boundaries is always less than or equal to the estimate from trace analysis. In figure 1(a), the boundaries marked with thick lines are coherent $\Sigma 3$ boundaries, while those marked by thin lines are non-CSL high angle boundaries. Such a distinction between $\Sigma 3$ and non-CSL high angle boundaries will be followed throughout the paper. The total length fraction of $\Sigma 9$

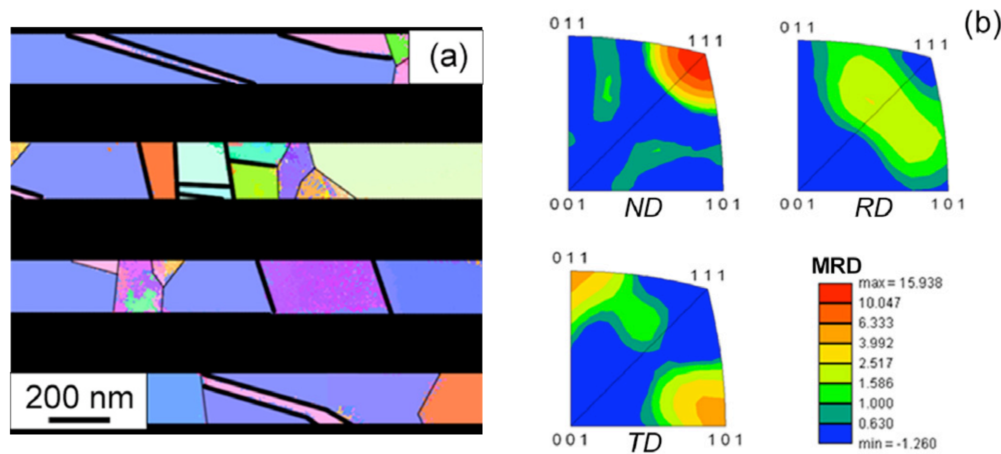

Figure 2. (a) Color coded IPF map from 180 nm wide Cu lines. Color codes for orientations are represented by the standard stereographic triangle in figure 1(a). (b) IPP show a strong bi-axial texture with ⟨111⟩ ∥ ND and ⟨110⟩ ∥ TD.

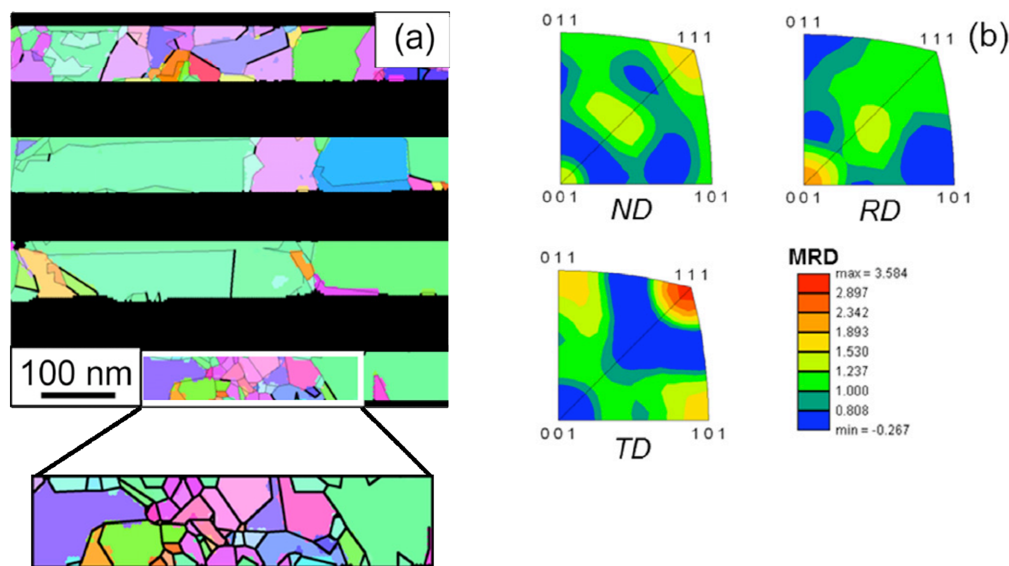

Figure 3. (a) Color coded IPF map from 120 nm wide Cu lines. Color codes for orientations are represented by the standard stereographic triangle in figure 1(a). In some regions, the microstructure consists of near bamboo-type grains in the vicinity of small grain clusters that mainly comprise high angle boundaries. A magnified image highlighting the cluster of small grains is shown at the bottom of (b). IPP show a slight ⟨111⟩ fiber texture along TD.

and $\Sigma 27$ boundaries was about 6%, while that of other CSL boundaries was negligible. Low angle boundaries categorized by the Brandon criterion [32] accounted for about 5% of the total boundary length. The results obtained are consistent with EBSD and XRD measurements carried out on 1.8 μm lines by Besser *et al* [19] and Cho *et al* [33].

A similar analysis was performed on narrower (180 and 120 nm wide) and periodic Cu line structures. Representative plan-view color coded inverse pole figure maps from these lines are shown in figures 2(a) and 3(a). The 180 nm CIs showed a prominent bi-axial texture with ⟨111⟩ ∥ ND and ⟨110⟩ ∥ TD (figure 2(b)). On the other hand, the 120 nm wide CIs revealed a slight ⟨111⟩ texture ∥ TD, as shown in figure 3(b). The microstructure of both sets of lines was bamboo-like [34]. Particularly in the case of 120 nm CIs, clusters of small grains were observed in the vicinity of large bamboo grains (figure 3(a)). The change in microstructure with line width for CIs is similar to earlier observations in Al interconnects [35]. It was also found that the total length fraction of coherent twin boundaries was higher in 180 nm CIs (25%) when compared with 18% for 120 nm lines. Furthermore, grain boundary character analysis carried out on data sets of about 10 000 boundaries for 180 and 120 nm wide lines showed that these coherent twin boundaries comprise more than 95% by length of all the $\Sigma 3$ boundaries present in these lines. $\Sigma 3^n$ ($n = 2, 3$) boundaries and low angle boundaries each accounted for less than 5% of the total boundary length.

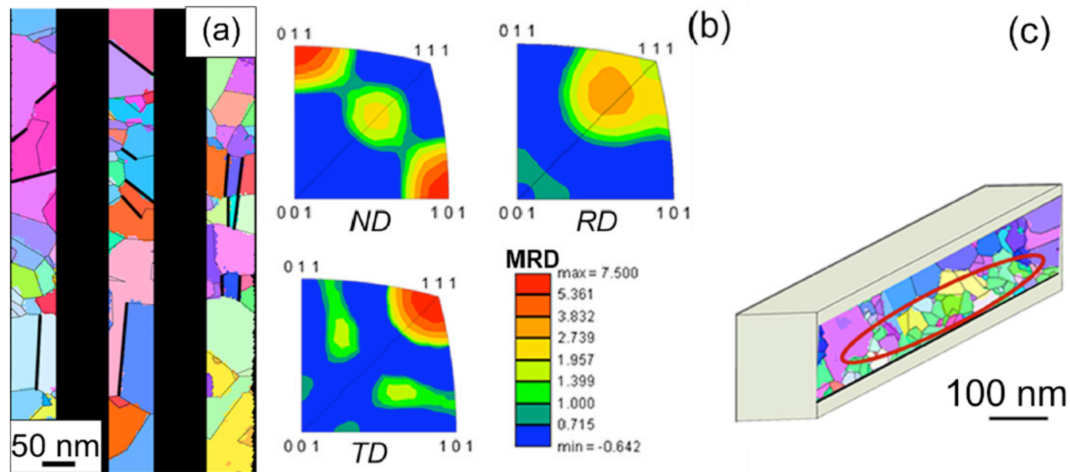

Figure 4. (a) Color coded IPF map from 70 nm wide Cu lines. Color codes for orientations are represented by the standard stereographic triangle in figure 1(a). The microstructure comprises clustered regions of small, nearly equiaxed grains sharing high angle boundaries in the vicinity of large bamboo-type grains and (b) IPP show strong ⟨111⟩ texture along the trench sidewall (TD), ⟨112⟩ ∥ RD and ⟨110⟩ ∥ ND. (c) Transverse cross section analysis also reveals clusters of small grains (highlighted in the figure by the red ellipse) at the trench bottom.

To investigate the effects of further downscaling on the microstructure, 70 nm wide Cu lines were analyzed. In contrast to the 180 and 120 nm CIs, the microstructure of the 70 nm CIs was polygranular (figure 4(a)). By definition, a polygranular microstructure is one in which there are continuous grain boundary paths along the length of the interconnect [36]. The crystallographic texture was found to be bi-axial with ⟨110⟩ along the trench depth and a dominant ⟨111⟩ along the trench width (figure 4(b)). The length fraction of coherent twin boundaries was also reduced to about 14%, while that of other CSL boundaries was less than 1%. Low angle boundaries constituted less than 5% of the total boundary length. Because CIs of this line width ($<$120 nm) are expected to show a dominant sidewall texture, transverse cross section analysis was also performed. The results also showed the presence of clusters of small equiaxed grains at the bottom of the trench, while larger grains appeared closer to the top of the trench (figure 4(c)).

The aforementioned results show that as the CI line width is reduced from 1.8 μm to 120 nm, the ⟨111⟩ fiber is weakened. In fact, 120 nm CI lines exhibit no normal texture, but show a slight preference for orientations where the {111} planes are parallel to the sidewalls, as first noted by Besser et al [19]. Such a texture becomes more severe in 70 nm wide lines, and can be attributed to sidewall grain growth [19]. In addition to this effect, the 70 nm CI lines have a strong preference for orientations where the ⟨112⟩ directions are along the line length, as also observed by Budiman *et al* [37]. Indeed, we observe a strong ‘brass’ component {110} ⟨112⟩. In addition to variations in texture, downscaling of CIs also results in changes to grain boundary characteristics. The length fraction of the coherent Σ3 boundaries decreases with decreasing line width (figure 5). Furthermore, the microstructure in narrower lines is polygranular with small grains separated by high angle boundaries.

To understand such microstructure variations upon downscaling, it is essential to note that CIs are dimensionally

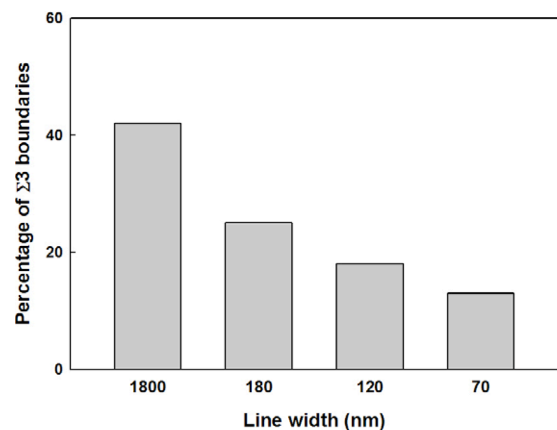

Figure 5. Variation in the length fraction of coherent Σ3 boundaries with CI line width.

constrained with multiple interfaces fabricated using complex processing conditions. Therefore, during the annealing process, grain growth is governed by multiple factors, which may be mutually competitive. The classical model assumes that, during grain growth, all boundaries move with velocities proportional to the average energy per unit area of the boundary and its average curvature [38]. However, in CIs, the grain growth process is more complex involving the minimization of surface energy, interfacial energy and strain energy contributions as well [38].

As CIs are downscaled, the surface and interface area to volume ratio increases. Thus, the surface and interfacial energy contributions become increasingly important during grain growth. Furthermore, with increasing aspect ratio (table 1), the area of the trench sidewall interface increases with respect to the trench bottom, which raises the influence exerted by the sidewall on the Cu grain structure. This leads to preferential growth of a sub-population of grains with crystallographically favorable orientations to minimize the

sidewall interfacial energy. Such an effect had previously been proposed by Thompson *et al* [38] and Harper *et al* [5]. To explore the favorable Cu orientations that minimize the total interfacial energy, it is important to recognize that the Ta diffusion barrier in contact with Cu deposited by the PVD process is the metastable phase β-Ta, having a tetragonal crystal structure. This has been experimentally confirmed through XRD by Wong *et al* [39]. With the β-Ta phase, Cu shares a hetero-epitaxial relationship such that the $[2\bar{2}0]$ direction on the (111) plane in Cu is parallel to the [330] direction on the (002) plane in Ta [39]. Therefore the growth of {111} Cu minimizes the energy of the Cu/Ta interface. In wider lines with lower aspect ratios, fiber textured grain growth with ⟨111⟩ along the trench normal minimizes the interfacial energy at the trench bottom. In narrower lines, though, the growth of the {111} grains growing perpendicular to the trench sidewall favors minimization of sidewall interfacial energy.

From a surface energy standpoint, for typical fcc metals such as Cu, the {111} surface energy (γ_{111}) is the lowest, with the ordering generally being ($\gamma_{111} < \gamma_{110} < \gamma_{100}$) for low Miller index planes [40]. Considering the case for CI trenches that have the bottom surface and sidewalls (with a Ta barrier) at 90° to each other, multiple scenarios can be derived for the combined minimization of surface energy and interfacial energy. From an energetics perspective, the ideal scenario would be a {111}/{111} type. However, crystallographically it is impossible to have two {111} planes perpendicular to each other. With these crystallographic limitations, the optimal grain orientation would be a {111}/{110} type. Therefore, the grains growing with ⟨111⟩ oriented along the trench normal would tend to align the ⟨110⟩ type direction along the trench sidewall to minimize both the surface and interfacial energy. This is consistent with our observations in wider lines. Similarly, the {111} grains growing normal to the trench sidewalls would have the {110} planes perpendicular to the trench normal. This is also consistent with the observed texture in narrow lines.

In wide lines (250 nm in width and above), it has been observed previously that during annealing, the grain growth process initiates in the overburden layer and propagates into the damascene trenches [41]. Therefore, the texture of the Cu grains in the trench is shown to be strongly dependent on the overburden. In some cases, almost complete invasion of the trench by the overburden has been observed, while in the other cases, twin boundaries have been shown to form where the invading grains from the overburden intersect the {111} grains growing bottom-up along the trench normal [22]. However, in narrow lines, the invasion of the overburden layer into the trench is restricted by the growth of sidewall {111} grains. The resulting microstructure is thus composed of clusters of small grains in the vicinity of some large grains. This phenomenon becomes more severe with reducing line width, thereby resulting in a polygranular structure as observed in 70 nm wide lines. In addition to these factors, in narrow lines, the {111} grains growing bottom-up are also restricted by the sidewall {111} grains. With increasing interface area to volume ratio, preserving both the configurations is important to minimize the overall interfacial energy. However, due to the increasing dominance of the trench sidewall at higher aspect ratios, and under the constraint that no two ⟨111⟩ directions in Cu can be perpendicular, clusters of small nearly equiaxed grains growing bottom-up remain trapped at the trench bottom.

CIs fabricated by the inlaid damascene process are also under mechanical stresses due to the difference in thermal expansion between the metallic interconnect and the substrate/dielectric that rigidly confines it, with the magnitude of these stresses being highest along the line length [19]. Therefore, to minimize the elastic strain energy, the Cu grains orient themselves in such a way that the direction with the lowest elastic modulus is aligned along the maximum stress direction. As copper has high elastic anisotropy [42], the elastic modulus is different along different crystallographic directions. The lowest elastic modulus is along the ⟨100⟩ direction ($E_{\langle 100\rangle} \sim 67$ GPa), while the highest is along the ⟨111⟩ direction ($E_{\langle 111\rangle} \sim 192$ GPa). The elastic modulus along any arbitrary direction $\langle hkl\rangle$ can be computed as

$$\frac{1}{E_{\langle hkl\rangle}} = \frac{1}{E_{\langle 100\rangle}} - 3\left(\frac{1}{E_{\langle 100\rangle}} - \frac{1}{E_{\langle 111\rangle}}\right) \times (\alpha^2\beta^2 + \beta^2\gamma^2 + \gamma^2\alpha^2) \quad (1)$$

where α, β, γ are direction cosines of $\langle hkl\rangle$. However, crystallographically, ⟨100⟩ directions cannot lie on {111} planes. Therefore, the sidewall-growing {111} grains align their two lowest elastic moduli directions present on the {111} planes, which are ⟨112⟩ and ⟨110⟩ along the directions of maximum principal stresses (namely the length and width of the CI line), to minimize the strain energy. The resulting textures in CIs obtained by minimizing the total energy are thus consistent with our results. In the specific case of sidewall growth of {111} grains, the ⟨112⟩ direction being aligned along the length of the line to minimize strain energy, results in a ⟨110⟩ normal texture, and consequently minimizes the surface energy as well.

The observation that small grains present in the interconnect microstructure seem to have nearly equiaxed structures separated by high angle boundaries instead of low energy coherent twin boundaries may be explained by topological effects restricting grain rotations [43]. For the nearly equiaxed grains sharing boundaries with many other grains, rotational changes to form specific low energy boundaries cannot occur in isolation since it may raise the total energy of the other system by increasing the energy associated with the other shared grain boundaries. Such reduction in the fraction of Σ3 boundaries with equiaxed grain structures has also been observed and predicted in the past by Gleiter *et al* [44] Randle [43] and Pande *et al* [45]. The presence of such small grain clusters in narrow lines increases the number of triple junctions and potential flux divergence sites. Concurrently, the presence of high angle boundaries between them may provide fast diffusion paths for mass transport, thereby affecting the electromigration reliability [34]. Large misorientations between grains in highly anisotropic Cu may also raise the level of local stresses, and when coupled with fast diffusion paths may deteriorate resistance to stress induced voiding.

4. Conclusions

The downscaling of damascene CIs strongly affects their microstructure, including grain texture, structure and grain boundary character. The microstructure evolution in dimensionally constrained narrow CIs is dependent on the growth of sidewall, bottom-up and overburden grains. In particular, the increasing influence of the trench sidewalls in narrow Cu lines results in dominant sidewall growth of {111} grains which orient themselves to minimize the surface energy and strain energy, thereby reducing the ⟨111⟩ fiber texture commonly observed in wider lines. The sidewall growth also obstructs the invasion the trench by the overburden grains and restricts the bottom-up growth of {111} grains. This results in a polygranular microstructure in narrow CIs with clusters of small grains at the trench bottom. Grain boundary trace analysis reveals that the fraction of coherent twin boundaries reduces with decreasing line width. The presence of such small grain clusters, mostly linked by high angle boundaries, may adversely influence stress migration and electromigration reliability in CIs. The experimental results shown herein on state-of-the-art interconnect structures provide evidence that microstructure evolution in narrow CIs is complex and strongly governed by a combination of factors including interface and strain energy. Further studies of local texture and grain boundaries on as-deposited structures, followed by grain evolution experiments and simulations during various annealing treatments, are necessary to completely understand and control the microstructure of CIs. Such investigations will be critical to fabricate interconnect structures with tightly controlled microstructures, low resistivity and enhanced reliability for future semiconductor metallization.

Acknowledgments

K J Ganesh and P J Ferreira acknowledge financial support from the Semiconductor Research Corporation (SRC), Task 2072.001, and valuable discussions with Professor Paul Ho at UT Austin. A Darbal and K Barmak gratefully acknowledge the financial support of the SRC, Tasks 1292.008 and 2121.001, and partial support from the MRSEC program of the NSF under DMR-0520425.

References

[1] Havemann R H and Hutchby J A 2001 *Proc. IEEE* **89** 586–609
[2] Rosenberg R, Edelstein D C, Hu C K and Rodbell K P 2000 *Annu. Rev. Mater. Sci.* **30** 229–62
[3] Kapur P, Chandra G, McVittie J P and Saraswat K C 2002 *IEEE Trans. Electron Devices* **49** 598–604
[4] Edelstein D *et al* 1997 *IEDM Tech. Dig.* 773–6
[5] Harper J M and Rodbell K P 1997 *J. Vac. Sci. Technol.* **15** 763–79
[6] Steinhogl W, Schindler G, Steinlesberger G, Traving M and Engelhardt M 2005 *J. Appl. Phys.* **97** 023706
[7] Carreau V, Maîtrejean S, Verdier M, Bréchet Y, Roule A, Toffoli A, Delaye V and Passemard G 2007 *Microelectron. Eng.* **84** 2733–9
[8] Knorr D B and Rodbell K P 1996 *J. Appl. Phys.* **79** 2409–17
[9] Campbell A N, Mikawa R E and Knorr D B 1993 *J. Electron. Mater.* **22** 589–96
[10] Knorr D B, Tracy D P and Rodbell K P 1991 *Appl. Phys. Lett.* **59** 3241–3
[11] Nucci J A, Shacham-Diamand Y and Sanchez J E Jr 1995 *Appl. Phys. Lett.* **66** 3585–7
[12] Nucci J A, Keller R R, Sanchez J E Jr and Shacham-Diamand Y 1996 *Appl. Phys. Lett.* **69** 4017–9
[13] Ryu C, Loke A L, Nogami T and Wong S 1997 *Proc. IEEE IRPS* pp 201–5
[14] Sun T, Yao B, Warren A P, Barmak K, Toney M F, Peale R E and Coffey K R 2009 *Phys. Rev.* B **79** 041402
[15] Meyers M A, Mishra A and Benson D J 2006 *Prog. Mater. Sci.* **51** 427–556
[16] Ganesh K J, Rajasekhara S, Zhou J P and Ferreira P J 2010 *Scr. Mater.* **62** 843–6
[17] Kim D, Paik J, Joo Y, Oh K H, Lee H and Dicks K 2002 *Mater. Sci. Forum* **408** 529–34
[18] Lee H J, Han H N and Lee D N 2005 *J. Electron. Mater.* **34** 1493–9
[19] Besser P *et al* 2001 *J. Electron. Mater.* **30** 320–30
[20] Lee D and Lee H 2003 *J. Electron. Mater.* **32** 1012–22
[21] Field D, Dornisch D and Tong H 2001 *Scr. Mater.* **45** 1069–75
[22] Brandstetter S, Carreau V, Maitrejean S, Verdier M and Legros M 2010 *Microelectron. Eng.* **87** 383–6
[23] Brandstetter S, Carreau V, Maitrejean S, Verdier M and Legros M 2010 *Scr. Mater.* **63** 965–8
[24] Ganesh K J, Kawasaki M, Zhou J P and Ferreira P J 2010 *Microsc. Microanal.* **16** 614–21
[25] Vincent R and Midgley P 1994 *Ultramicroscopy* **53** 271–82
[26] Rauch E F and Dupuy L 2005 *Arch. Metall. Mater* **50** 87–99
[27] Own C S, Marks L D and Sinkler W 2006 *Acta Crystallogr.* A **A62** 434–43
[28] Moraweic A and Bouzy E 2006 *J. Appl. Cryst.* **39** 101–3
[29] Rauch E F and Dupuy L 2006 *J. Appl. Cryst.* **39** 104–5
[30] Wright S I and Larsen R J 2002 *J. Microsc.* **205** 245–52
[31] Helmick L, Dillon S J, Gerdes K, Gemmen R, Rohrer G S, Seetharaman S and Salvador P A 2011 *Int. J. Appl. Ceram. Technol.* **8** 1218–28
[32] Brandon D G 1966 *Acta Metall. Mater.* **14** 1479–84
[33] Cho J Y, Mirpuri K, Lee D N, An J K and Szpunar J K 2005 *J. Electron. Mater.* **34** 53–61
[34] Walton D T, Frost H J and Thompson C V 1992 *Appl. Phys. Lett.* **61** 40–2
[35] Knowlton B D, Clement J J and Thompson C V 1997 *J. Appl. Phys.* **81** 6073–80
[36] Fayad W R, Andleigh V K and Thompson C V 2001 *J. Mater. Res.* **16** 413–6
[37] Budiman A S, Besser P R, Hau-Riege C S, Marathe A, Joo Y C, Tamura N, Patel J R and Nix W D 2009 *J. Electron. Mater.* **38** 379–91
[38] Thompson C V 2001 *Solid State Physics* vol 55 (Burlington: Academic)
[39] Wong S, Ryu C, Lee H and Kwon K 1998 *Mater. Res. Soc. Proc.* **514** 75–81
[40] Sanchez J E Jr, Besser P R and Field D P 1998 *AIP Conf. Proc.* **418** 230–5
[41] Jiang Q, Nowell M, Foran B, Frank A, Havemann R, Parihar V, Augur R and Luttmer J 2002 *J. Electron. Mater.* **31** 10–5
[42] Courtney T 2000 *Mechanical Behavior of Materials* (New York: Mcgraw-Hill)
[43] Randle V 1996 *The Role of Coincient Site Lattice in Grain Boundary Engineering* (Cambridge: University Press)
[44] Gleiter H 1969 *Acta Metall.* **17** 1421–8
[45] Pande C S, Imam M A and Rath B B 1990 *Metall. Trans.* A **21** 2891–6